Estimations of Global Warming Potentials from Complete Ab Initio Calculations for CH_2F_2 Verified by Comparison to Experiment

Paul Blowers

Department of Chemical and Environmental Engineering

The University of Arizona

PO Box 210011

Tucson, AZ 85721-0011

blowers@engr.arizona.edu Ph: 520-626-5319 Fax: 520-621-6048

Abstract

In this work, the global warming potential of methylene fluoride is estimated through purely computational chemistry methods. We find our computational chemistry approach reproduces well all phenomena important for predicting global warming potentials. Geometries predicted using the B3LYP/6-31g* method were in good agreement with experiment, although some other computational methods performed slightly better. Frequencies needed for both partition function calculations in transition state theory, and infrared intensities needed for radiative forcing estimates, agreed well with experiment compared to other computational methods. A modified CBS-RAD method used to obtain energies led to superior results to all other previous heat of reaction estimates and most barrier height calculations when the B3LYP/6-31g* geometry optimization method was used as the base structure. The Wigner tunneling correction and the harmonic oscillator approximation led to accurate reaction rate constants and radiative forcing estimates without requiring any experimental data. Atmospheric lifetimes from theory at 277 K were indistinguishable from experimental results, as were the final global warming potentials compared to experiment. This is the first time complete ab initio methods have been applied to estimate a global warming potential for a chemical and we have found the approach to be robust, inexpensive, and accurate compared to prior experimental results.

Introduction

Global warming is a scientifically based environmental impact incurred due to industrial, consumer, and natural processes. As awareness of global warming became apparent through the development of global warming potential (GWP) analyses, the Kyoto Protocol was introduced and signed by nearly every industrialized country to control emissions of six compounds into the atmosphere that contribute largely to planetary warming. The six compounds that are covered by the protocol are[1]: CO_2, CH_4, N_2O, SF_6, HFCs, and PFCs. This paper will investigate the GWP of one HFC, CH_2F_2, also known as HFC-32, using only quantum chemical methods, and will compare intermediate results and final GWPs to experimental data to demonstrate computational chemistry is a viable way of achieving high quality results.

A general formula for GWP regarding trace gases like the one in this work is[2-4]:

$$GWP_i = \frac{\int_0^{TH} a_i [x_i(t)] dt}{\int_0^{TH} a_{ref} [x_{ref}(t)] dt} \qquad (1)$$

where TH is the time horizon for GWP the species will be considered over, a_i is the radiative forcing due to a unit increase in atmospheric concentration of species i, $[x_i(t)]$ is the time dependent concentration of a pulse of species i, while the corresponding quantities for a reference gas are in the denominator. Typically, the TH is chosen to be 20, 100, or 500 years[3,5]. So, GWP estimates for chemical species are generally based on the atmospheric lifetime of the compound released into the environment, the radiative forcing due to the absorption of energy in the 700 to 1500 cm^{-1} range[6-8], and the concentration of the species[9]. Figure 1a shows the information needed and the flow of information transfers to reach global warming potential estimates through experiment.

The time dependent concentrations of the species can only be known through degradation reaction rates and adsorption rates onto particulates or solids, the latter of which are relatively small and will be ignored in this work[10]. The first part of the results section will focus on generating the kinetic parameters leading to accurate $x_i(t)$'s for the species through quantum mechanical determination of rate constants as a function of temperature.

Radiative forcing, a_i, can be found through experiments[3,11] or theory[12] and requires IR spectra and cross sections for the species of interest[13]. The second section of the results will demonstrate how to estimate this phenomena, while the final section will present the theoretically predicted GWP.

Carbon dioxide is often chosen as the reference gas, meaning any change in the predicted CO_2 concentrations over the TH may lead to changes in the GWP_i. This is why some advocate using only the numerator of the GWP_i as the index instead of referencing it to CO_2, calling this the absolute GWP ($AGWP_i$). In this work, we will compute the numerator and use published CO_2 data to convert to GWP_i so comparisons can be made to prior results[13].

GWP are available for few chemicals[3] although estimates are continually being developed for new species. The small number of available GWPs is due to the complexity of both the kinetic experiments and the difficulty in carrying out the radiative forcing measurements using high quality cross-sections measured through IR experiments[8,13]. Recent work is still populating data bases regarding radiative forcing[14] while many CFC replacement materials have yet to be evaluated[15]. And with large data differences among research groups for all of the pieces of information going into the GWP estimation, there can be large variations in GWP from one work to another[13].

This work uses only theoretical chemistry methods and handles every step of predicting global warming potentials with those techniques, as shown in Figure 1b. This is the first time that a complete series of calculations for GWP prediction using these methods has been done for any species, highlighting the utility of quantum chemical methods for obtaining high quality data when experiments are difficult or expensive to carry out.

Choice of species

Methylene fluoride, CH_2F_2 (HFC-32), is investigated because there is much data available in each category needed to demonstrate that quantum chemical methods can be robustly applied to predict all parts of global warming potential estimates. The availability of data in each category is listed next while the quality of the data is deferred until the results and discussion section.

Although CH_2F_2 is not listed on the US Environmental Protection Agency (US EPA) Toxic Release Inventory (TRI)[16], and emissions are difficult to estimate, this species has experimental data to allow us to use the species as a benchmark species. It is true that other halogenated compounds are emitted into the atmosphere in higher quantities, like HFC-23 and HFC-134a[17]. However, CH_2F_2, is used as a replacement material for CFCs[18] and has important commercial usage as a fire extinguishant [19,20]. This use is noteworthy because it is one of the chemical uses where the substance is chosen specifically to be emitted to the environment during its use. More uses are as a refrigerant[21] or in the manufacture of other organic products[22].

Availability of kinetic data for comparison

Hydroxyl reaction with atmospheric pollutants containing carbon-hydrogen bonds is the primary mechanism for degradation of the chemicals[23]. Although several studies have been done on the kinetics of hydroxyl radical with CH_2F_2[20,24-31], there are some discrepancies among the data. Not all of the data covers the same temperature range, and there is little data available at the low temperatures that are encountered in the troposphere where degradation occurs. It is particularly important to note the discrepancies become larger at lower temperatures where there is little data available[32]. This is the region where extrapolations fail because of non-Arhennius curvature, indicating extrapolations of data from higher temperatures may fail[32]. Additionally, there are difficulties in measuring highly accurate rate constants for reactions of hydroxyl radicals with other species, as highlighted in detail by Kurylo and Orkin[32] and by Wayne, et al[33]. While Kurylo and Orkin state that ab initio work may be equal to the difficulty of obtaining experimental results and that the analyses require experimental data[32], this paper will show the direct application of robust quantum chemical methods to evaluate GWP leading to evaluations of kinetics, radiative forcing, and global warming potential that are indistinguishable from experimental results. With these caveats detailed, we'll chronologically consider each of the experimental kinetic data sets.

Howard and Evenson[25] did early measurements of many halogen substituted methane molecules using a discharge flow reactor while monitoring the presence of hydroxyl radical using laser magnetic resonance detections. Their measurement for CH_2F_2 was done only at 296 K with pressures between 107 and 1200 Pa. Pressure should not affect the reaction rate since it is a bimolecular reaction and they found this to be true. Using 12 different experiments, they determined the reaction rate to be $7.8\pm1.2\times10^{-15}$ cm^3/molecule sec.

Clyne and Holt[27] followed up on this original work using resonance-fluorescence detection of hydroxyl radicals in a similar discharge flow system. They measured reaction rates from 293 K to 425 K and found the rate to be $7.2\pm1.0\times10^{-15}$ cm^3/molecule sec at 298 K. They also fit their results using an Arhennius type plot.

Nip, et al.[26], measured the hydroxyl radical reaction rates for many fluorinated alkanes at 297 K and found a reaction rate of 1.13×10^{-14} cm^3/molecule sec for CH_2F_2. They examined their results and suggested secondary reactions during their flash-photolysis resonance-absorption investigation may contribute errors as much as 10% to their measurements.

Jeong and Kaufman[24] measured the reaction rate of hydroxyl with chlorinated and fluorinated methanes between 250 and 480 K. They found non-Arhennius behavior for all substances except CHF_3, highlighting why

some extraporations of Arhennius-type equations may not represent real phenomena outside the temperature range where data is collected. Like most experiments, they carried their work out under pseudo-first order conditions where the concentration of CH_2F_2 was much higher than the hydroxyl radical concentration and found the rate would be represented by:

$$k\left(\frac{cm^3}{molecule\,sec}\right) = 7.31x10^{-12}\,T^{1.95}\,\exp\left(-\frac{2.23\frac{kcalK}{mol}}{RT}\right). \qquad (2)$$

Bera and Hanrahan[30] used an argon-based radiolysis-absorption spectroscopy technique and a relative rate method at room temperature. This is a method where one injects two separate reactants into the reactor and then monitors changes in the disappearance of the hydroxyl radical over time. One then uses knowledge of the other reactant's kinetic rates to calculate the reaction rate for the species of interest. They describe some of the experimental difficulties they overcame, especially the need to increase the fluorinated species concentrations to avoid problems with the presence of water. They measured a rate of $8.8x10^{-15}$ cm^3/molecule sec at room temperature

Talukdar, et al.[29], used discharge flow-laser magnetic resonance combined with a pulsed photolysis-laser induced fluorescence technique between 222 and 393 K to find the reaction rate for the reaction studied here. They measured low amounts of impurities, primarily CH_3CF_3 at concentrations less than 20 ppmv and were careful to minimize the effect of the impurities. They also realized that products of the first degradation step could affect the further disappearance rates of hydroxyl radical. They used a lower initial OH concentration to prevent this from affecting their results. They found a kinetic rate constant between 1.96 and 30.43 $x10^{-15}$ cm^3/molecule sec over the temperature range of interest.

Hsu and Demore[28] measured rate constants for 15 hydroxyl radical reactions with halogen-substituted alkanes. They used a temperature range between 283 and 403 K using a relative rate technique and UV photolysis of a hydroxyl precursor. Since direct photolysis can cause complications, they were careful to reduce difficulties by measuring rate constant ratios for more than one reference compound. Like some of the previous research, they chose to fit their kinetic rates to an Arhennius function without realizing there could be curvature in the plot at lower temperatures. Their expression is:

$$k\left(\frac{cm^3}{molecule\,sec}\right) = 1.8x10^{-12}\exp\left(-\frac{1552K}{T}\right) \qquad (3)$$

leading to a rate constant of $9.8x10^{-15}$ cm^3/molecule sec at room temperature.

Szilagyi, et al.[31], did the most recent study to measure the reaction rate of CH_2F_2 with hydroxyl radical. They performed discharge flow resonance fluorescence experiments only at 298 K and found a rate constant of $1.00x10^{-14}$ cm^3/molecule sec. They monitored the disappearance of hydroxyl radical in this case, like many of the other research prior to theirs. They also mentioned that the presence of impurities could lead to an overestimation of the rate constant, even though they used high purity chemicals.

DeMore[34] did an evaluation of the kinetic data available up to 1994 and came up with an Arhennius form for the reaction rate:

$$k\left(\frac{cm^3}{molecule\,sec}\right) = 1.9x10^{-12}\exp\left(-\frac{1550K}{T}\right) \qquad (4)$$

There have been many computational chemistry studies of the hydrogen abstraction by hydroxyl reaction for CH_2F_2, much as there have been many experimental studies. Bottoni, et al., performed the first ab initio calculations for the reaction using the lower level of theories commonly available at that time[35]. They reported molecular structures compared to experiment and also reported activation energies and heats of reaction. We will compare to their work for the structures later, but will only mention their energies in passing here since their work was limited to the computational methods available in the early 1990s.

Jursic[36] followed the original work by using B3LYP/6-31g(2d,2p) calculations to find the transition state for the hydrogen abstraction reaction. While he computed the barrier height for this and several other reactions, he did not continue on to estimate reaction kinetics using transition state theory so we will only be able to use his results for comparison for some parts of our work.

Schwartz, et al.[20], did quantum chemical calculations of the kinetic rates for this reaction using HF/6-31g* frequencies and MP2(full)/6-31g* optimized structures. They used transition state theory (TST) and found that tunneling was overestimated by Eckart tunnelling functions. To correct for this, they proceeded to calculate a higher level energy surface for the tunnelling effect at the G2 level of theory. They found that tunneling was reduced because of a broader barrier at the higher level of theory, yet were still unable obtain agreement with experimental values at low temperatures. Instead of investigating their methodology to obtain high level computational energies,

they instead empirically changed their energy barrier to yield agreement with experiments. This approach will not work for other cases unless experimental data for new chemicals is available.

Korchowiec, et al.[37], investigated several hydrofluoromethane degradation reactions using a modified Gaussian-2 energy calculation. They computed reaction rates from 280 to 420 K, which does not go low enough in temperature to investigate the reaction rate at temperatures commonly encountered in the troposphere. However, they extensively tested different computational methods and basis sets for predicting heats of reaction . Including the same tunneling correction we describe in our methodology section, they estimated reaction rates using transition state theory by using a free rotor approximation for the lowest transition state frequency as opposed to assuming the harmonic oscillator approach we will use. Unfortunately, the authors did not report their rate constant results, instead choosing to report only the activation energies abstracted from their calculations. The predicted barrier heights were in fairly good agreement with experiment at 298 K as we will see in the results and discussion section.

Louis, et al.[38], performed calculations for 12 partially halogenated methanes using geometry optimizations at the MP2/6-311g(2d,2p) level while following up with higher level energy calculations that did not include any composite energy methods. They applied transition state theory using the same methods we will introduce while also using the same Wigner tunneling correction. In their work, they compared reaction enthalpies, energy barriers, and kinetic rate constants only at 298 to experiment. They found they were within a factor of 2 of the experimental results at 298 K.

Gonzalez-Lafont, et al.[39], performed calculations using variational transition state theory for the reaction from 200 to 500 K. They included tunneling at low temperatures using a large-curvature ground state methodology and used a variety of single point energy calculations combined with different geometry optimization methods ranging from semi-empirical PM3 calculations to QCISD/6-31g* results. Despite all the different computational combinations they attempted, they were unable to reproduce experimental data at low temperatures compared to the data of Talukdar, et al.[29] In our methodology, we will describe a non-variational approach for obtaining the kinetic rates that gives excellent results for this reaction. We suspect the authors did not include the structure factor, did not include thermal corrections to the activation energy, and did not include the more minor corrections to switch to enthalpy from the internal energy or electronic energy calculations they used.

Finally, El-Taher[40] did the most recent calculations for the reaction of interest, surprisingly at some of the lowest levels of calculation, UHF/6-31g* and MP2/6-31++g*. The author reported many optimized structures and

energies at different levels of theory. While testing 13 different computational energy calculations, he only obtained agreement with experiment for the barrier height when using extremely large basis sets. The heats of reaction, unfortunately, performed less accurately compared to those in this work. This author also did not compute reaction rates from their energetics using transition state theory so only limited comparisons to those results will be available in the results section.

Now that all of the available experimental and computational kinetic and reaction transition state theory information has been described, the availability of spectroscopic information regarding species involved in the evaluation of this work will be highlighted.

Availability of IR data for comparison

There are several experimental measurements available for the IR spectra of CH_2F_2[18,21,41-43] and several predictions using quantum chemistry[41,44-46]. We will not discuss details of the spectroscopy other than listing some of the experimental difficulties and the prior computational work.

There are many experimental difficulties that need to be overcome in order to get high quality spectra for determining radiative forcing, especially in the far infrared region[18]. Experimental errors may come from many sources including inadequate instrumental resolution[47], sample (backward) emission, sample impurities, including water[14], temperature control, pressure measurements, pathlengths, photometric errors, systematic equipment errors, and adsorption. While some of these errors can be minimized through good experimental design, the errors can lead to differences in integrated absorption coefficients of about 30%[18].

Previous computationsinvolved work at a variety of levels and used both scaled and unscaled frequencies. It is well known that most computational methods overpredict IR vibrational frequencies so scaling factors are often used to compensate and allow prediction of high quality frequencies[48,49]. More about this will be detailed in the methods section. Wang, et al., used the correlated MP2 method with unrestricted calculations using the cc-pVDZ basis set and scaled their results[41]. Zachariah used HF/6-31g* scaled frequencies[46], Amos used MP2/6-31g unscaled frequencies[44], and Fox and Schlegel in their extensive testing of computational methods used calculations up to the MP2/6-311++g(3d,3p) level[45]. A comparison of vibrational frequencies from experiment and theory to those in this work will be done in the results section to demonstrate the viability of our selected computational methods.

Availability of IR intensities:

It is unusual for experimentalists to report IR intensities. However, a few have been measured[43,50,51] or predicted from computations[44,52] for CH_2F_2. Morcillo, et al.[51], were the first to report infrared intensities for the species of interest when they used a pressure broadening technique combined with two separate spectrophotometers with a variety of crystalline materials. In their work, they reported intensities for 8 of the 9 frequencies. Kondo, et al.[43], then investigated Coriolis interactions at 11 atm using FT-IR with a resolution of 0.5 cm^{-1}. They reported most band intensities, but were unable to separate intensities at 1090, 1111, and 1178 cm^{-1}, instead aggregating them as one intensity. Their convention of summing these three intensities will be followed in this work when comparison is made to their results.

For computational work, Bunnell, et al.[52], used the CNDO/2 method and predicted the infrared intensities using a semiempirical method. Fox and Schlegel[45] followed many years later with a comprehensive testing of computational method and basis set combinations for predicting both vibrational frequencies and infrared intensities. They found the infrared intensities were more sensitive to basis set choice than vibrational frequencies were, but one does not observe any obvious trends in improvement as one increases basis sets or levels of electron correlation. Amos, et al.[44], then did extensive testing one year later and used the MP2/6-31g method to predict both infrared frequencies and intensities. They went on to add anharmonic corrections to their results.

All experimental and computational infrared intensities are compared to the work done here in the results section.

Availability of radiative forcing estimates

In order to compare the species in this work to radiative forcing experimental values, we list previous results here. Pinnock, et al., reported the earliest value for radiative forcing for CH_2F_2 and did extensive testing of some approaches for approximating high quality results[11]. They measured the absorption spectra for 18 halocarbons, including the first reported integrated absorption cross section measurement for CH_2F_2. Use of their narrow band model with different atmospheric conditions yielded an instantaneous cloudy radiative forcing of 0.129 W/m^2 ppbv and a clear sky radiative forcing of 0.182. We will compare mostly to the former cloudy sky radiative forcing number in later sections of this work. Pinnock, et al., then created a simplified model discussed in the methodology section where one can directly translate absorption cross sections to radiative forcing without doing the complex atmospheric modeling previously needed. They found errors between full model results and simplified band model of around one percent.

Papasavva, et al.[12], followed up on the simplified model from Pinnock and created an extension that uses ab initio data to replace the experimentally determined absorption cross sections. They performed calculations for 20 halogenated organic species using MP2 calculations with a 6-31g** basis set and obtained a value of 0.115 W/m^2 ppbv for CH_2F_2.

Naik, et al.[15], extensively examined kinetic rates of degradation reactions to build a large data set of atmospheric lifetimes for halocarbons. They also went on to build a consistent set of radiative forcings for 21 species using a full atmospheric model. They found an instantaneous radiative transfer value of 0.148 W/m^2 ppbv compared to a WMO value of 0.13[53]. In the same year, Jain, et al.[54], evaluated radiative forcings for 39 greenhouse gases, many of them for the first time. They used both narrowband and broadband radiative transfer models through highly intensive computer simulations of atmospheric interactions. They estimated the instantaneous cloudy sky radiative forcing to be 0.168 W/m^2 ppbv with the narrowband model and 0.149 with the broadband model. Highwood and Shine[3] measured absorption cross sections for 11 species and used their data to obtain a cloudy sky radiative forcing of 0.11 W/m^2 ppbv. As discussed later, they used a scaling factor to calculate a lifetime adjusted forcing of 0.09 W/m^2 ppbv. Further testing showed that neglecting the intensities below the normal atmospheric window would introduce some error, which is why we include these intensities in our estimate.

Sihra, et al.[14], followed up the previous work to evaluate 65 halocarbons and hydrocarbons. They performed line-by-line model calculations of atmospheric interactions to predict a constant profile cloudy sky radiative forcing of 0.114 W/m^2 ppbv. Lifetime adjusted results were reported to be 0.105 W/m^2 ppbv. Gohar, Myhre, and Shine added more data to the growing body of literature through both a narrow band model and a line-by-line radiative transfer model. They found a cloudy sky instantaneous radiative transfer value of 0.110 W/m^2 ppbv. More recent work by Gohar, et al.[17], reports instantaneous clear sky radiative forcing of 0.143, instantaneous cloudy sky radiative forcing of 0.110 and adjusted cloudy values of 0.121.

Radiative forcings are available for relatively few species compared to the number of chemicals that are in industrial use, even though more are being measured and modeled as time goes on. And for species where many values have been predicted like CH_2F_2, there are discrepancies among the predictions. Experimental determination of radiative forcing involves many uncertainties, including the assumed atmospheric composition, cloudiness, and spectroscopy measurements[55]. A recent study of CF_3CH_2F using different atmospheric models with several sets of experimental cross sections found that even the best predictions would only agree to within 12-14%[17,56]. Other

work suggests errors may be as much as 25%[13]. This shows that quantum chemical predictions that are within 14% of experimental data will confirm that the theoretical predictions, at least for radiative forcing, are indistinguishable from experimentally based values. Again, quantum chemical calculations will not suffer from the experimental difficulties so estimation of radiative forcing may be more robust and repeatable within the limitations of the quantum chemical calculations.

Availability of GWP from experimental values

There are several sources of GWP values for CH_2F_2 based on experimental values and the development of values for species parallels that of radiative transfer models. Pinnock, et al.[11], Used an atmospheric liftime of 6.0 years to obtain global warming potentials of 0.47, 0.18, and 0.16 for 20, 100 and 500 year time horizons using CFC-11 as a reference substance. To convert these to values that can be compared to others, we use the GWPs relative to CO_2 for CFC-11 reported by Naik[15] and Jain[54] to estimate Pinnock's GWPs relative to CO_2. The average GWPs relative to CO_2 for CFC-11 are 6067, 4725, and 1704 at time horizons of 20, 100, and 500 years. This yields GWPs relative to CO_2 of 2851, 851, and 273 from Pinnock's results. Similarly, Highwood and Shine found GWP relative to CFC-11 of 0.321, 0.133. and 0.118 using an atmospheric lifetime of 5.6 years. This gives GWP relative to CO_2 of 1947, 628, and 201.

For the rest of the results, the GWPs have been calculated using CO_2 as the reference species so the previous transformations are not needed. Naik, et al.[15], used an atmospheric lifetime of 5.6 years to obtain GWPs of 3500, 1100, and 350 at the commonly used THs. Jain, et al.[54], used an atmospheric lifetime of 5.28 years to find GWPs of 2920, 889, and 276. Sihra reports the GWP only at 100 years to be 710 using at atmospheric lifetime of 5.6 years[14].

Most recently, Orkin, et al.[47], measured IR absorption cross sections for several haloalkanes and then detailed a new scaling method for obtaining global warming potentials by comparing results to CFC-11 as a reference species. They obtained GWP of 1800, 580, and 170 using an atmospheric lifetime of 5.4 years.

Wuebbles[57] based his GWP results on WMO[53] and IPCC results. However, neither of those sources details the information leading to their results in detail and it would be difficult to verify methods or intermediate calculations. However, Wuebble's summary yields GWPs of 1800, 580, and 180 at TH's of 20, 100, and 500 years, respectively.

Note that none of the above works reported the source or value of the CO_2 reference data so it is not clear how to evaluate the quality of these data sets. This uncertainty occurs because the CO_2 reference data is constantly being reevaluated. We recommend that all GWP results using CO_2 as the reference species explicitly report the CO_2 reference data to allow intercomparisons among data sets.

Now that we have introduced all of the data that can be used to validate our results at each step of calculation, we will discuss the methodologies applied in this work.

Methods

Theoretical Calculations

In this work, the Gaussian98 software package[58] was used to perform all of the quantum mechanical calculations. The choice of computational method and basis set greatly affects the quality of computational chemistry work. We have found[59-61] that the choice of basis set and method for the geometry optimization and frequency calculations is less important than the choice of energies used for rate constant estimation. Due to the lesser expense of density functional calculations and our past work reproducing experimental geometries, we used the B3LYP method combined with the 6-31g* basis set for geometry optimizations and frequency calculations. This is a slightly smaller basis set than that of Lei's previous work on atmospheric chemistry reactions[62], yet has given us and others[63] excellent structures that do not change significantly when even much larger basis sets are used[64]. Further justification for our basis set and method choice comes from analyses of vibrational frequency accuracies showing that our choice is the most accurate of the extensively tested Density Functional Theory (DFT) methods[49]. This is important because we use vibrational frequencies in our rate constant estimations and in radiative forcing predictions.

Several past papers used quantum chemical calculations to predict infrared intensities which are needed for radiative forcing estimates[8]. The inclusion of electron correlation was found to be important for X-H band intensities for a host of smaller species[8,44,65-67], which is why we selected the B3LYP method; it is one of the better DFT methods including a correlation functional[68]. More extensive testing was done by Hall and Schlegel where they found the hybrid density functional methods were more accurate in reproducing IR intensities compared to high level calculations and experiment than HF, MP2, non-local, or gradient-corrected methods[69]. They also tested the effect of basis set choice on predicting IR intensities. As one moved from small basis sets to larger ones, 6-31g* had already captured most of the improvement possible compared to enlarging the basis set to 6-311+g(3df,3pd). Other

work has shown that polarization is important as well[65,67], which is why the 6-31g* basis set was chosen; since we will soon be studying much larger molecules, the smallest viable basis set was chosen here. Based on the previous work, we are confident that our IR intensities will be accurate enough to lead to radiative forcing results that are indistinguishable compared to experimental results.

All stable structures were verified to be the correct structures through frequency calculations where minima had no negative eigenvalues and the first order transition state had one negative eigenvalue corresponding to the reaction mode. An intrinsic reaction calculation was done on the adiabatic energy surface to ensure the transition state linked the correct reactants to the correct products since complex energy surfaces can be difficult to investigate with just a frequency calculation. Frequencies were scaled by a factor of 0.9613[49] because this reduces the RMS error of predictions compared to experiments to 34 cm^{-1}, and the need for scaling factors is well documented for this substance[45]. The scaling factor of Scott and Radom leads to slightly higher errors with an RMS error of 45 cm^{-1} so it was not chosen in this work[48]. Zero point energies (ZPE) were scaled by 0.98256[70].

Much of our work for radical species[59,71] has found that the CBS-RAD method[72] is very reliable for heats of reaction and activation energies. This is because the large basis sets include polarization and the methods include correlation, which have both been found to be important for some halogenated species[73]. While other work on predicting halogenated organic reaction energetics[74] used the G2-(MP2,SVP) method, that method has not been validated to accurately predict activation energies. We have shown that a modified CBS-RAD[60,61] method reproduces activation energies to within a few kcal/mol consistently so we used this methodology. Also, this composite method should remove some of the errors associated with spin contamination found in similar reactions[75].

In addition to using the high quality CBS-RAD composite energy method, zero point energies and thermal corrections were included for all species[76]. The harmonic oscillator approach was used for all vibrations to determine the thermal corrections. For barrier heights, the change in the the number of moles times the gas constant times temperature was added to the internal energy results to convert to enthalpy.

Transition State Theory:

Our reaction is bimolecular so rate constants are calculated using traditional transition state theory with the following expression[77]:

$$k = \frac{k_b T}{h} \kappa L \frac{Q_{TS}}{Q_{OH} Q_{CH_2F_2}} \exp\left(\frac{-E_a}{RT}\right) \qquad (5)$$

where Q_{OH}, $Q_{CH_2F_2}$, and Q_{TS} are the complete translational-vibrational-rotational-electronic partition functions for the reactants and the transition state, respectively. L is the statistical factor, which is 2 in this case since there are two equivalent hydrogens that can be abstracted, k_b is Boltzman's constant, h is Plank's constant, E_a is the barrier height, R is the gas constant, and T is temperature in degrees Kelvin.

Tunneling is a quantum effect where reactant molecules that do not have enough energy to cross the barrier can still sometimes react. Tunneling effects can be calculated with the Wigner correction[78]:

$$\kappa(T) = 1 + \frac{1}{24}\left(\frac{h\nu c}{k_b T}\right)^2 \qquad (6)$$

where c is the speed of light; ν is the imaginary frequency that accounts for the vibrational motion along the reaction path; and $\kappa(T)$ is the tunneling coefficient.

Radiative Forcing:

Instantaneous radiative forcing has been defined as[11]:

$$F_{tot} = \sum_{i=1}^{250} 10\sigma_i F(\upsilon_i) \qquad (7)$$

where the spectra from 0 to 2500 cm^{-1} has been separated into 10 cm^{-1} bins, σ_i is the measured infrared (IR) cross section, and $F(\nu_i)$ is the radiative forcing for the species in that bin. While cross sections and radiative forcing functions can be found experimentally, they can also be obtained through quantum mechanical calculations. Particularly, a simplification of the above formula leads to[12]:

$$F_{tot} = \sum_{k} A_k F(\upsilon_k) \qquad (8)$$

where A_k is the IR intensity evaluated for peak k. In reference [12], the authors used the MP2/6-31g** method and basis set and found results with this simplified methodology were within 3% of the complete method of Pinnock[11]. The authors used the harmonic oscillator approach, which we will also use since the lower frequency results where hindered rotors might be found will not change the results significantly. While overtone spectra and dipole moment functions can be calculated with ab initio methods[79-85], these results appear to contribute less than 10% to the final GWP[6,12,86] so this complexity will be ignored in this work.

In addition, Freckleton, et al.[87], showed that moving from the extremely computationally demanding line-by-line method of radiative forcing evaluation to the narrow-band-method used in this work would not lead to errors

greater than 10%, even for species like CF_4 where this comparison would be most sensitive. Again, this is within the 14% error expected for even the highest quality model results. This justifies the use of the 10 cm^{-1} bin procedure we followed. While the atmospheric window between 700 to 1500 cm^{-1} [6-8]has been used extensively, research has shown that lower vibrational modes may also contribute to radiative forcing[18]. In this work, we expand the work of Elrod[9] and Papasavva[12] to encompass the lower frequency contributions down to 0 cm^{-1}.

Atmospheric Lifetime Estimation:

One can estimate atmospheric lifetimes of species by multiplying the global atmospheric lifetime of a reference compound that is well characterized, often chosen to be CH_3CCl_3, by the ratio of the OH reaction rate constant at 277 K for CH_3CCl_3 to that for a new species[88,89]:

$$\tau_{\text{lifetime, R}} = \tau_{\text{lifetime, CH}_3\text{CCl}_3} \times \frac{k_{\text{OH + CH}_3\text{CCl}_3}(277\text{K})}{k_{\text{OH + R}}(277\text{K})} \qquad (9)$$

Here, the data from DeMore[90], *et al*., was used to estimate the rate constant of CH_3CCl_3 at 277 K to get a value of 6.686×10^{-15} cm^3/molecule-sec[88]. While Kurylo and Orkin suggest a temperature of 272 be used[32], we will stick to the more common convention of 277 K. Because the reaction rate of species with the hydroxyl radical is dependant on the hydroxyl radical concentration, it is important to know that value to a high degree of accuracy. Unfortunately, analyses using many techniques give differences of 20 to 30% for the hydroxyl radical concentration[32], suggesting that atmospheric lifetimes may have similar differences.

The atmospheric lifetime of CH_3Cl_3 has been modeled to be 4.8 years[91], but other work suggests it should be 5.9 years[32]. We will use a more recent value of 5.7 years in our work [15].

Results and Discussion

Molecular Geometries

Geometries optimized using our basis set and method are compared to other results in Table 1 to gain insight into the quality of the basis set and method used in this work. Unfortunately, we were unable to secure a copy of reference 14 of ref [92] in this work so we rely on their transcribed experimental information. However, several other data sets have been included in Table 1.

In order to evaluate the computational methods used in this work, we select the most recent work of Hirota[93] as the benchmark. The error estimate they report is 0.0005 Angstroms for the C-F bond length and 0.003 Angstroms for the C-H bond length. This gives an average error of 0.00175 for the expected error in experimental

bond length measurements. Any results that are within these bounds would be indistinguishable from experimental results.

We see the B3LYP/6-31g* results in this work lead to an average bond length error of 0.011 Angstroms, and that only one method, CCSD(T)/cc-pVQZ, gives errors within the experimental expectation, with an average error in bond length of 0.0012 Angstroms. Ten other methods other than ours yield average bond length errors less than the ones from B3LYP/6-31g* calculations, and most of these use much larger basis sets like cc-pVTZ or 6-311++g** combined with higher level and more expensive methods. The other five methods yield higher errors than ours and are mostly lower level methods with much smaller or equivalent basis sets. Again, one of our goals is to prove B3LYP/6-31g* performs adequately for all predicted phenomena for GWP estimation. The secondary goal is to use the smallest basis set and lowest level method that gives accurate results so we may evaluate much larger species in our future work. We see that, to these ends, the B3LYP method has lower errors than HF or MP2 results. It is puzzling in some of the comparisons to see three works[45,46,94] used the same method and basis set but yield different reported results. However, some of these results may be slightly skewed because of rounding differences.

Comparing angles, our work leads to an average error of 0.615 per angle comparing only the FCF and HCH angles, which are the two available angles in Hirota's work. We should note that Hirota estimated the average absolute error of their measurements to be 0.18 degrees. No predictions fall within this experimental range, with only the CID/6-31g* results being just out of range. All but the semiempiricle CNDO methods, however, perform better than the basis set and method chosen in this work with average absolute errors ranging between 0.19 and 0.555 degrees. We will see that while the geometries may not be the highest accuracy from our methods, they will be accurate enough to reproduce spectroscopic information and give structures accurate enough for use in the composite CBS-RAD method to yield high quality reaction barrier results.

Table 1 - A comparison of geometry parameters for CH_2F_2 from the B3LYP/6-31g* geometry optimization in this work to previous computational and experimental results. All bond lengths are in Angrstroms while angles are listed in degrees.

Geometry Parameter (Source]=)	This work	expt [41]	expt., ref 14 from [92]	expt. [95]	expt. [93] Improved from ref [95]	expt. [96]	MNDO results [94]	HF/ 3-21g [94]
R_{C-F}	1.361		1.3508	1.357±0.001	1.3508±0.0005	1.358±0.001	1.309	1.341
R_{C-H}	1.096	1.093	1.084	1.093±0.003	1.084±0.003	1.092±0.003	1.085	1.059
A_{HCF}	108.86						123.30	122.50
A_{FCF}	109.14	108.30	108.49	108±3	108.49±0.06	108±6		
A_{HCH}	112.22	113.70	112.80	113±10	112.8±0.30	111±25		
average error in bond length (Angstroms)	0.011	N/A	N/A	N/A	0.0	N/A	0.021	0.017
average error in angle (degrees)	0.615	N/A	N/A	N/A	0.0	N/A	N/A	N/A

Geometry Parameter [Source]	CNDO/2 [52]	CID/ 6-31g* [45]	HF/ 6-31g* [45]	QCISD/ 6-311++g** [92]	MP2/ 6-311++g** [92]	MP2/ 6-11+g* [92]	MP2/ 6-31g [44]
R_{C-F}	1.348	1.353	1.338	1.358	1.360	1.361	1.366
R_{C-H}	1.122	1.087	1.078	1.092	1.090	1.089	1.091
A_{HCF}				108.70	108.50	108.60	108.60
A_{FCF}	105.20	108.67	108.60	108.40	108.60	108.60	108.60
A_{HCH}	111.36	112.60	112.46	113.40	113.60	113.80	113.70
average error in bond length (Angstroms)	0.020	0.003	0.009	0.008	0.008	0.008	0.011
average error in angle (degrees)	2.365	0.19	0.225	0.345	0.455	0.555	0.505

Geometry Parameter [Source]	MP2/ 6-31g* [37]	CCSD(T)/ cc-pVQZ [39]	HF/ 6-31g* [94]	B3LYP/ cc-pVTZ [97]	HF/6-31g* [46]	UMP2(full)/ cc-pVDZ [41]	B3LYP/ 6-311g** [37]
R_{C-F}	1.363	1.351	1.310	1.361	1.338	1.359	1.364
R_{C-H}	1.093	1.086	1.063	1.091	1.078	1.093	1.091
A_{HCF}	108.70	108.50	122.60	N/A	108.90	108.90	108.80
A_{FCF}	108.80			108.6523		108.90	108.90
A_{HCH}	113.30	113.09		113.1839	112.50	112.30	112.80
average error in bond length (Angstroms)	0.011	0.001	0.031	0.009	0.009	0.009	0.010
average error in angle (degrees)	0.105	0.288	N/A	0.273	0.3	0.455	0.205

There is no experimental data for the structure of the CHF_2 radical. However, all of the calculations are in good agreement with each other other than the HF/6-31g* results which underpredict the bond lengths. Even the cc-pVDZ results with the MP2 method here are in agreement with our less computationally demanding method and basis set, as shown in Table S1. As there is no experimental data available for this species, the data is summarized in the supplementary information. We will follow this convention throughout this work since the specialized data may be of interest to only select readers. Likewise, Table S2 and S3 show geometry optimizations and frequency results for the transition state from this work compared to all previous works as there is no experimental data to use as a benchmark.

Vibrational frequencies and intensities

Table S4a in the supplementary information shows a summary of infrared peak locations from our predictions compared to experimental and other computational work. Figure 2 shows a summary of the predicted frequency locations versus the experimental information. For comparison, we will use the results of Smith[21], Wang[41], Suzuki[42], and Kondo[43], as the benchmark since they show excellent experimental agreement through independent measurements. Using these experimental results, we find an average absolute error in frequency prediction of 17.0 cm^{-1} using the scaled B3LYP/6-31g* results, 22.9 for MP2/cc-pVDZ, 13.8 for HF/6-31g*, 62.4 for MP2/6-31g*, and 64.67 for MP2/6-311g(3d,3p) predictions. Our result is within the expected error of 34 cm^{-1} normally expected for our method and basis set[49].

The results of Zachariah, et al.[46], used HF/6-31g* results and scaled them similarly to our methodology. Surprisingly, they found an average absolute error of 13.8 cm^{-1} for the CH_2F_2 species when this method normally has slightly larger errors. We, however, find our results are well within the expected errors for scaled results and that only one other predicted data set matched well with experimental values.

A very extensive testing of basis set effects on the accuracy of vibrational frequencies was done by Bruns, et al.[67] and they found that MP2/6-311++g** gave the best agreement compared to experiment with an average error of 37.0 cm^{-1}. Clearly, our scaled frequencies show less error than 37.0, again justifying our choice of computational method and basis set compared to the more expensive calculations.

It is not just the location of the vibrations that are important, but also the IR intensities must be accurate in order to predict radiative forcing correctly. Fortunately, by choosing CH_2F_2, there are several experimental data sets available for comparison to our predictions in this work. The work of Kondo, et al.[43], and others are compared with

our work and earlier experiments in Table S4b in the supplemental information. Figure 3 shows a plot of the predicted intensities versus the experimental ones. Direct comparison of calculated and experimental intensities is difficult due to overlap among some of the bands[45], which is why some of the results in Table S4b have been lumped together.

One of the discussion threads in Smith, et al.'s[21], work showed temperature did not significantly affect the integrated cross sections of the species, normally leading to changes of about 10% over almost a one hundred degree change in temperature. Much of this change was due to a change in the overtone spectra, which already contribute little to the radiative forcing. Due to this finding, we use the infrared intensities and vibrational frequencies calculated at the default Gaussian98 temperature of 298.15 K.

Bruns, et al.[67], extensively tested the MP2 method with a wide variety of basis sets and found there was no trend in accuracy for predicting IR intensities as one increased the basis set. This demonstrates that just moving to a higher level of theory may not lead to improved results. In their case, they found that MP2/6-311++g, MP2/6-31++g, HF/6-31g, and HF/6-311g calculations performed the best with errors of 12.1, 12.8, 17.8, and 19.3 km/mol respectively. In our work, our errors compared to the same experimental data [43] yield an average error of 23.12 km/mol. We see our method of choice compares very favorably to the larger basis sets and more expensive combinations of their evaluative work. The earlier semi-empirical work of Bunnell, et al.[52], though, gives much higher errors of 103.0 km/mol. The results of Fox, et al., lead to errors of 16.0 km/mol, which is slightly better in performance than our method. On the other hand, very large basis sets with MP2 calculations can reduce the error to 3.1 km/mol[45], but these calculations would be too expensive to carry out on the larger species of interest in our future work. We will see in a later section how the errors in intensity do not greatly affect the radiative transfer estimates so our choice of computational method and basis set is adequate.

Heat of Reaction

Heats of formation are readily available for CH_2F_2 (-107.71 kcal/mol), OH (9.319 kcal/mol), and H_2O (-57.799) in the NIST webbook[98], a continuation of the well used JANAF tables. However, the heat of formation for CHF_2 is not as readily available. Four results are available in the literature and they are -57.1[99], -55.7[94], -58.6[100], and -59.2[101] kcal/mol. In addition, computational work using the BAC-MP4 method suggests the heat of formation should be -59.11 kcal/mol[46] with an uncertainty around 2 kcal/mol. The same methodology showed the heat of formation of CH_2F_2 would be 107.8 kca/mol suggesting this latter value may be correct.

Using an intermediate value of -57.65 kcal/mol for the CHF_2 radical heat of formation, we calculate an experimental heat of reaction of -17.06 kcal/mol. This is compared to the predicted results using the CBS-RAD method and B3LYP/6-31g* geometry optimization where we get a heat of reaction of -16.86 kcal/mol. Our error is only 0.2 kcal/mol.

Louis, et al.[38], computed the heat of reaction at the PMP4(SDTQ) level with the 6-311g(2d,2p) and 6-311++g(3df,3pd) basis sets and got results of -17.73 and -16.25 kcal/mol respectively. El-Taher reported heats of reaction that ranged between 9.93 kcal/mol and -16.31 kcal/mol[40], with several clustered near -16 kcal/mol using the highest levels of theory in that work. The work of Korchowiec found a value of -18.4 kcal/mol[37].

One can see that we obtain the best agreement with experimental values considering how large the differences are for the heat of formation of the CHF_2 radical. The other predicted heats of reaction all perform worse than our method. This again demonstrates the CBS-RAD method performs excellently in estimating reaction energetics, as we have repeatedly found before[60,61,71].

Barrier Height

A comparison of barrier height is not particularly useful[76] unless it is done at a single temperature where high quality data is available because of the strong curvature in many of the hydroxyl hydrogen abstraction reaction kinetic plots. Table 2 shows a comparison of barrier heights at 298.15 K from a host of experimental and theoretical works.

Table 2 - A comparison of predicted barrier heights compared to experiment. All barrier height results are compiled at 298.15 K to facilitate comparison due to the curvature in the log k versus 1/T plot. For computational results, all method listings are (energy level//geometry optimization level)

E_a (kcal/mol)	Method(ref)
3.61	CBS-RAD//B3LYP/6-31g* This work
3.52	Experimental[24]
3.10	Experimental[28,90]
27.44	UHF/3-21g*// UHF/3-21g*[35,a]
31.15	UHF/6-31g*[40]
2.19	MP2/3-21g*// UHF/3-21g*[35,a]
5.91	PMP2/6-31++g*//UHF/6-31g*[40]
6.07	G2/MP2(max) - no ZPE[20]
6.86	Eckart Potential fit of G2 results[20]
2.1	B3LYP/6-311g(d,p) [102]
3.70	PMP4(SDTQ)/6-311g(3df,2p)//MP2/6-311g(2d,2p) [38]
3.56	PMP4(SDTQ)/6-311++g(3df,3pd)//MP2/6-311g(2d,2p) [38]
0.1	B3LYP/6-311g(2d,2p) [36]

[a]ZPE included, thermal corrections included. Additionally, conversion to enthalpy from internal (electronic energy) was included, as in this work.

The very low barrier height of this reaction prevented some errors from becoming apparent in comparison to experiments, as errors tend to show up as the barriers get larger. MP2 is known to overestimate activation energies[36], but does not in this case. However, this overestimation is apparent with the HF results, which also overpredict activation energies[36]. Likewise, DFT methods, including B3LYP tend to give activation barriers that are too low[36,103-105]. Based on our experience, we hypothesize that these deviances only become apparent when activation energies are greater than about 15 kcal/mol, which is why the errors may not be appearing here.

It is surprising that the work of Louis, et al.[38], gives results that are comparable in quality to the CBS-RAD results reported here. Apparently, their basis set was large enough to compensate for the lower level method used in their work. However, they did include all of the thermal, zero point, and energy corrections to obtain an enthalpy, which most of the other works have not done. Also, their approach uses a much larger geometry optimization method and basis set with MP2/6-311g(2d,2p) calculations. We are interested in estimating GWPs for much larger molecular systems so their approach would not be applicable for those species. All other barrier heights reported by other researchers show worse agreement compared to experimental values than our methodology, again justifying our choice of basis set, method, and composite energy method.

Rate Constants from Transition State Theory

A comparison of the current and past work to predict rate constants for the degradation of CH_2F_2 is shown in Figures 4 and 5. We see in Figure 4 that the experimental data from Jeong, et al.[24], lies lower than any of the other results, while there are several sets of data that overlap about one order of magnitude larger. As discussed earlier, the experiments are very challenging for these reactions, and this is shown by the order of magnitude difference.

Looking at Figure 5, we see that our data lies exactly on top of the experimental data. Schwartz, et al[20], using G2 energies showed large errors at low temperatures. They found that with the Eckart energy barrier they still underpredicted the reaction rate, especially at lower temperatures. To compensate for this, they scaled their activation energy to the experimental value and were then able to reproduce the experimental data. While this methodology seems attractive, it would preclude being able to predict reaction kinetics accurately for new species since they relied on correcting their activation energy to match experimental data, which is why their results appear to match the DeMore[34] compiled correlation well. If they did not have experimental data available to do this empirical fitting, they would have had much larger errors.

The other previous computational work shows larger deviations at low temperatures and has errors throughout the entire temperature range. This work is the first computational work that correctly predicts reaction rates for this reaction. One can recall our methodology and that there are no empirical fittings needed, no barrier shifting, no unusual tunneling approaches, and we did not have to treat the hindered rotor as such. While this may appear to be a fortuitous cancellation of errors that leads to such outstanding agreement with experimental results, we have consistently found our methodology to work for a wide range of reactions[59-61,106].

Louis, et al.[38], performed calculations at the PM4(SDTQ) level with two large basis sets and found they always overpredicted the rate constant between 250 and 400 K. They treated the rotation about the C-H-OH axis as a hindered rotor, which should have improved their results over the harmonic oscillator approach we have used. They also used the same Wigner tunneling correction used in this work. Their barrier heights, too, are between 3.5 and 3.7 kcal/mol so they are in very good agreement with experiment, like our results. It is not clear why their rate is a half order of magnitude higher than the experimental data across the temperature range when so many of their intermediate results agree with our results and experiment.

Gonzalez-Lafont, et al.[39], did further work on the reaction using a variety of computational methods and basis sets. They used the semiempirical PM3 method for their primary geometry optimization method but computed energies at higher levels of theory and also with composite energy methods. They computed rate constants using a variety of tunnelling corrections using transition state theories of several types including variational methods. They found their energy surface did not appear to represent the reaction coordinate well at the low PM3 level[39] and needed to include variational methods, the presence of weak van der Waals complexes in the reactant channel, and complex tunnelling corrections to improve their results, even with the high quality composite energy methods. Unfortunately, they were still unable to reproduce rate constants from Talukdar, et al.[29], at low temperatures even with all of these corrections. They ended their work by concluding more work is needed in order to understand why transition state theory appears to fail for this reaction. We have found, though, that our methodology agrees well with experiment at all temperatures and our data can be used to directly estimate the atmospheric lifetime of CH_2F_2, which is performed in the next section.

Atmospheric lifetime:

Atmospheric lifetimes are one important contribution for differentiating the environmental impacts of chemicals. While the stratospheric lifetime of a species cannot be simplified as easily as the tropospheric lifetime,

research has shown that the inclusion of stratospheric contributions is often a small correction to the tropospheric lifetime[32], which is why we do not include stratospheric degradation in this work. The predicted kinetic rate through TST is 6.269×10^{-15} cm^3/molec-sec at 277 K. The preferred value of 5.7 years for τ,CH_3CF_3[15], leads to an atmospheric lifetime of 6.08 years for our reaction of interest. This is compared to other published values in Table 3.

Table 3 - Atmospheric lifetime, τ, for CH_2F_2 compared to other evaluations. τ is in units of years.

τCH_2F_2 (years)	Source
6.08	This work
5.40	Naik, et al. [15] using a Prather and Spivakovsky scaling
5.4	Reference 39 from Orkin, et al. [47]
5.6	Jain, et al.[3,54] secondary reference
6.8	Prather, et al. [89]full atmospheric model
7.3	Prather, et al. [89] scaled results using approximation
6.0	Wuebbles [57] from WMO[53] and IPCC grey literature

We find that our atmospheric lifetime is only 0.11 years away from the average of all other previously reported atmospheric lifetimes. Again, our methodology is robust enough to lead to results that are indistinguishable from experimental ones.

We now turn to our estimate for radiative forcing using Pinnock's bin method, combined with Papasavva's ab initio transformation. It should be noted that, following the work of Papasavva[86], we ignored the absorption overtone spectra because inclusion contributes a small percentage effect on the radiative forcing. In Table 4 we compare our predicted radiative forcing values to those of other researchers. It should be noted that these radiative transfer values are not scaled for atmospheric lifetime.

Table 4 - Instantaneous radiative transfer evaluations for CH_2F_2 (in W m^{-2} ppb^{-1}) prior to incorporating lifetime correction factors.

F_{CH2F2} (W/m^2 ppbv)	% error compared to source data	Source
0.121	N/A	This Work
0.148	-18	Naik, et al. [15] full atmospheric model
0.11	+10	Highwood, et al. [3] narrow band model
0.13	-7	WMO, [53] unclear methodology
0.129	-6	Pinnock, et al. [11] narrow band model
0.121	0	Gohar, et al. [17] adjusted cloudy model
0.168	-28	Jain, et al.[54] narrow band model
0.149	-23	Jain, et al. [54] broad band model
0.173	-30	Jain, et al.[54] narrow band model with global and annual average mean background atmosphere
0.114	+6	Sihra, et al. [14] line by line
0.115	+5	Papasavva, et al. [12] from ab initio methods

A comparison of errors compared to the previous results for radiative forcing shows our result here predicts a radiative forcing that is six percent lower than Pinnock's[11] more extensive work, but one that is 5 percent higher than Papasavva's[12] earlier compuational chemistry work. Our result is 18 percent lower than Naik's work[15], which is

about four percent outside of the range discussed earlier regarding the average difference among even the best radiative transfer estimates from experiment. Jain[54] did multiple estimates and all three are higher than any of the other estimates, suggesting their results may not represent true behavior. Our errors compared to that work range from 23 to 30 percent. Compared to Highwood and Shine[3], our result is only higher by ten percent, indistinguishable from their results. We are also only 15 percent higher than Sihra's work[14]. Compared to Gohar, et al.[17], our predictions match perfectly with their results based on a full line-by-line model of atmospheric interaction for adjusted cloudy sky values.

If we discard Jain's results which appear to be significantly higher than all other radiative forcing estimates, we find an average value of 0.122 W/m2 ppbv. Our predicted result is 0.121, which is in excellent agreement with the average from complex atmospheric modeling and computationally demanding approaches. This is the last information needed to predict GWPs which we do in the next section.

Global Warming Potential

The atmospheric lifetime can be combined with radiative forcing to obtain global warming potentials. Instead of using equation 1, we shift to the atmospheric lifetime based formulation to get[9]:

$$GWP_i = \frac{a_i \int_0^{TH} e^{-\frac{t}{\tau}} dt}{AGWP_{CO_2}(TH)} \qquad (10)$$

where we use the AGWPs at 20, 100, and 500 year time horizons for the CO_2 reference species previously introduced from Wuebble's work[57].

If atmospheric lifetimes are longer than 200 years, one can use the radiative forcing directly to estimate GWP. However, Highwood and Shine[3], pointed out that one should scale the radiative forcing by a multiplicative factor when the atmospheric lifetimes are shorter. In our case, with an atmospheric lifetime less than 10 years, the radiative forcing needs to be multiplied by 0.8 before performing the GWP calculation. However, not all previous work was scaled the the atmospheric lifetime. It should be noted that all GWP have been scaled by an explicit comparison to the GWP of CO_2,, as discussed in the introduction. While the AGWP of CO_2 may vary by up to 20% depending on the model used, we follow the work of Wuebbles and use GWPs of CO_2 equal to 0.235, 0.768 and 2.459 W yr/m^2 ppmv at TH's of 20, 100, and 500 years, respectively[57]. This will allow us to scale our GWP results

for comparison to other GWP's estimated from experimental results. We break Table 5 up into two segments to allow us to fairly compare to previous GWPs from experimental methods.

Table 5- Global Warming Potential Estimates for CH_2F_2 Compared to Literature Values. Convert to AGWP using the WMO CO_2 GWPs.

GWP_{20}	GWP_{100}	GWP_{500}	Source
3019	959	300	This Work
2851	851	273	Pinnock, et al. [11]
2920	889	276	Naik, et al. [15]
3500	1100	350	Jain, et al. [54]
	880		WMO [53]
Atmospheric lifetime adjusted values[a]			
GWP_{20}	GWP_{100}	GWP_{500}	Source
2415	768	240	This Work
1800	580	170	Orkin, et al. [47]
	710		Sihra, et al. [14]
1800	580	180	Wuebbles [57]
1947	628	201	Highwood, et al. [3]

[a] results have been scaled by atmospheric lifetime following Highwood and Shine[3].

We integrate the AGWP and we find a predicted GWP of 3019 at 20 years, 959 at 100 years, and 300 at 500 years. If we use Highwood's method[3] of scaling for atmospheric lifetimes, we obtain 2415, 768, and 240 for these same time horizons, respectively. Pinnock's[11] results, which were not scaled for atmospheric lifetime, are in excellent agreement with our unscaled results, with differences of less than 13% at each time horizon. Again, there have been no overall comparisons of how accurate GWPs are from one study to another. We would argue that since the radiative forcing cannot be measured more accurately than within fourteen percent[56] that GWPs also cannot be reproduced more accurately than that; we are within that limit, even disregarding all other sources of experimental or computational error.

Similar analyses show that we have an average error of four percent compared to Naik[15] and a nine percent error compared to WMO values[53] at a 100 year time horizon. Orkin's work is a little more problematic as it introduces a new methodology and compares GWP directly to CFC-11 in many areas. We conclude from the magnitude of their numbers that they have actually computed a scaled result for atmospheric lifetime, although it is not clear how all the details played out during their analyses.

Jain's perceived overestimates of radiative forcing compared to all other works suggest their GWP will be higher, and they are at all time horizons. No statistics were done to compare to their work since their results are significantly higher than other researchers. Sihra reported a value only at 100 years and their results were scaled by an atmospheric lifetime correction. We differ from their results by only eight percent.

Wuebble's results predate the introduction of the atmospheric lifetime scaling for radiative forcing and come from two other compilations of data. It is unclear whether these were unscaled or scaled results but the magnitudes suggest they were atmospheric lifetime scaled. Compared to our similar results, we find errors of 33 percent. While this may be outside the minimum error expected if only radiative forcing caused errors, we claim our results are indistinguishable from experiment since Pinnock and Wuebble also disagree substantially. Finally, Highwood and Shine[3] used scaled results that were higher than those of Wuebbles and our error compared to those results is 21 percent on average.

Conclusions

We find throughout this work that our computational chemistry approach accurately reproduces all phenomena important for predicting global warming potentials. Geometries predicted using the B3LYP/6-31g* method were in good agreement with experiment. Frequencies needed for both partition functions in transition state theory calculations, and infrared intensities needed for radiative forcing estimates, agreed well with experiment compared to other computational methods. The CBS-RAD energies used in this work were superior to all other previous heat of reaction estimates and most barrier height calculations when the B3LYP/6-31g* geometry optimization method was used as the base structure. The Wigner tunneling correction and the harmonic oscillator approximation led to accurate reaction rate constants and radiative forcing estimates without requiring any experimental data. Atmospheric lifetimes from theory at 277 K were indistinguishable from experimental results, as were the final global warming potentials compared to experiment. This is the first time complete ab initio methods have been applied to estimate a global warming potential for a chemical and we have found the approach to be robust, inexpensive, and accurate compared to prior experimental results.

Supporting Information Available: Geometry information for the radical product, CHF_2 appears in Table S1 compared to previous computational work. Complete geometry information results for the transition state from this work and from other reported works appear in the supporting information as Table S2. A summary of transition state frequencies used in the partition functions for the transition state theory calculations also appear in Table S3. Table S4a contains detailed numerical data used to make Figure 2, while the information for Figure 3 is in Table S4b. References to all information that appears in these supplementary tables also appears at the end of the material. The material is available free of charge via the Internet at http://pubs.acs.org

References:

(1) United Nations Environment Programme: environment for development; United Nations Environment Programme, 2005.

(2) Lashof, D. A., Ahuja, D. R. *Nature* **1990**, *344*, 529.

(3) Highwood, E. J., Shine, K. P. *J. Quant. Spectroscopy Radiat. Transfer* **2000**, *66*, 169.

(4) Houghton, J. T. Climate change, 1994 : radiative forcing of climate change and an evaluation of the IPCC IS92 emission scenarios; University Press: New York, NY, 1995.

(5) Albritton, D. L. D., R. G.; Isaksen, I. S. A.; Lal, M.; Wuebbles, D. J. Trace Gas Radiative Forcing Indicies. In *Climate Change 1994*; Hougton, J. T., Meira Filho, L. G.; Bruce, J.; Lee, H.; Callandar, B. A.; Haites, E.; Harris, N.; Maskell, K., Ed.; Intergovernmental Panel on Climate Change, Press Syndicate of the University of Cambridge: New York, NY, 1995; pp 205.

(6) Papasavva, S., Illinger, K. H.; Kenny, J. E. *J. Phys. Chem.* **1996**, *100*, 10100.

(7) Sidebottom, H., Franklin, J. *Pure Appl. Chem.* **1996**, *68*, 1757.

(8) Clerbaux, C., Colin, R.; Simon, P. C.; Granier, C. *J. Geophys. Res.* **1993**, *98*, 10491.

(9) Elrod, M. J. *J. Chem. Educ.* **1999**, *76*, 1702.

(10) Khalil, M. A. K., Rasmussen, R. A. *Env. Sci. Pollut. Res.* **2000**, *7*, 79.

(11) Pinnock, S., Hurley, M. D.; Shine, K. P.; Wallington, T. J.; Smyth, T. J. *J. Geophys. Res. Atmos.* **1995**, *100*, 23227.

(12) Papasavva, S., Tai, S.; Illinger, K. H.; Kenny, J. E. *J. Geophys. Res.* **1997**, *102*, 13643.

(13) Fuglestvedt, J. S., Berntsen, T. K.; Godal, O.; Sausen, R.; Shine, K. P.; Skodvin, T. *Climatic Change* **2003**, *58*, 267.

(14) Sihra, K., Hurley, M. D.; Shine, K. P.; Wallington, T. J. *J. Geophys. Res. Atmos.* **2001**, *106*, 20492.

(15) Naik, V., Jain, A. K; Patten, K. O.; Wuebbles, D. J. *J. Geophys. Res* **2000**, *105*, 6903.

(16) E.P.A., U. S. U.S. Environmental Protection Agency, Toxic Release Inventory, 2005.

(17) Gohar, L. K., Myhre, G.; Shine, K. P. *J. Geophys. Res. Atmos.* **2004**, *109*, D01107.

(18) Beukes, J. A., Niclaisen, F. M. **2000**.

(19) *Kirk-Othmer Concise Encyclopedia of Chemical Technology*, 4th edition ed.; John Wiley & Sons, Inc.: New York, NY, 1999.

(20) Schwartz, M., Marshall, P.; Berry, R. J.; Ehlers, C. J.; Petersson, G. A. *J. Phys. Chem. A* **1998**, *102*, 10074.

(21) Smith, K., Newnham, D.;Page, M.;Ballard, J.;Duxbury, G. *J. Quant. Spectroscopy Radiat. Transfer* **1996**, *56*, 73.

(22) Hydrofluorocarbons (HFC) Difluoromethane HFC-32.

(23) Atkinson, R. *Chem. Rev.* **1985**, *85*, 69.

(24) Jeong, K.-M., Kaufman, F. *J. Phys. Chem.* **1982**, *86*, 1808.

(25) Howard, C. J., Evenson, K. M. *J. Chem. Phys.* **1976**, *64*, 197.

(26) Nip, W. S., Singleton, D. L.; Overend, R.; Paraskevopoulos, G. *J. Phys. Chem.* **1979**, *83*, 2440.

(27) Clyne, M. A., Holtz, P. M. *J. Chem. Soc. Faraday Trans. 2* **1979**, *75*, 582.

(28) Hsu, K.-J., DeMore, W. B. *J. Phys. Chem.* **1995**, *99*, 1235.

(29) Talukdar, R., Mellouki, A.; Gierczak, T.; Burkholder, J. B.; McKeen, S. A.; Ravishankara, A. R. *J. Phys. Chem.* **1991**, *95*, 5815.

(30) Bera, R. K., Hanrahan, R. J. *Radiat. Phys. Chem.* **1988**, *32*, 579.

(31) Szilagyi, I., Dobe, S.; Berces, T. *React. Kinet. Catal. Lett.* **2000**, *70*, 319.

(32) Kurylo, M. J., Orkin, V. L. *Chem. Rev.* **2003**, *103*, 5049.

(33) Wayne, R. P., Canosa-Mas, C. E.; Heard, A. C.; Parr, A. D. *Atmos. Environ.* **1992**, *26A*, 2371.

(34) DeMore, W. B. *Chemical kinetics and photochemical data for use in stratospheric modeling [microform] : evaluation number 11*; Jet Propulsion Lab, NASA: Pasadena, CA, 1994.

(35) Bottoni, A., Poggi, G.; Emmi, S. S. *J. Molec. Struct. (Theochem)* **1993**, *279*, 299.

(36) Jursic, B. S. *Chem. Phys. Lett.* **1996**, *256*, 603.

(37) Korchowiec, J., Kawahara, S.; Matsumura, K.; Uchimaru, T.; Sugie, M. *J. Phys. Chem. A* **1999**, *103*, 3548.

(38) Louis, F., Gonzalez, C. A.; Huie, R. E.; Kurylo, M. J. *J. Phys. Chem. A* **2000**, *104*, 8773.

(39) Gonzalez-Lafont, A., Lluch, J. M.; Espinosa-Garcia, J. *J. Phys. Chem. A* **2001**, *105*, 10553.

(40) El-Taher, S. *Int. J. Quant. Chem.* **2001**, *84*, 426.

(41) Wang, B., Hou, H., Gu, Y. *J. Phys. Chem. A* **1999**, *103*, 9049.
(42) Suzuki, I., Shimanouchi, T. *J. Molec. Spectrosc.* **1973**, *46*, 130.
(43) Kondo, S., Nakanaga, T.; Saeki, S. *J. Chem. Phys.* **1980**, *73*, 5409.
(44) Amos, R. D., Handy, N. C.; Green, W. H.; Jayatilaka, D.; Willets, A.; Palmieri, P. *J. Chem. Phys.* **1991**, *95*, 8323.
(45) Fox, G. L., Schelegel, H. B. *J. Chem. Phys.* **1990**, *92*, 4351.
(46) Zachariah, M. R., Westmoreland, P. R.; Burgess, D. R. Jr.; Tsang, W.; Melius, C. F. *J. Phys. Chem.* **1996**, *100*, 8737.
(47) Orkin, V. L., Guschin, A. G., Larin, I. K., Huie, R. E., Kurylo, M. J. *J. Photochem. Photobiol. A: Chem.* **2003**, *157*, 211.
(48) Scott, A. P., Radom, L. *J. Phys. Chem.* **1996**, *100*, 16502.
(49) Wong, M. W. *Chem. Phys. Lett.* **1996**, *256*, 391.
(50) Mizuno, M., Saeki, S. *Spectrochim. Acta A* **1976**, *32*, 1077.
(51) Morcillo, J., Zamorano, L. J.; Heredia, J. M. V. *Spectrochim. Acta* **1966**, *22*, 1969.
(52) Bunnell, J., Crafford, B. C.;Ford, T. A. *J. Molec. Struct.* **1980**, *61*, 383.
(53) "WMO Scientific Assessment of Ozone Depletion. World Meteorological Organisation,", 1999.
(54) Jain, A. K., Briegleb, B. P.; Minschewaner, K.; Wuebbles, D. J. *J. Geophys. Res. Atmos.* **2000**, *105*, 20773.
(55) Pinnock, S., Shine, K. P. *J. Atmos. Sci.* **1998**, *55*, 1950.
(56) Forster, P. M. d. F., Burkholder, J. B., Clerbaux; C., Coheur; P. F., Dutta, M.; Gohar, L. K.; Hurley, M. D.; Myhre, G.; Portmanss, R. W.; Shine, K. P.; Wallington, T. J.; Wuebbles, D. *J. Quant. Spectroscopy Radiat. Transfer* **2005**, *93*, 447.
(57) Wuebbles, D. J. *Annu. Rev. Energy Environ.* **1995**, *20*, 45.
(58) Frisch, M. J., G. W. Trucks; H. B. Schlegel; G. E. Scuseria; M. A. Robb; J. R. Cheeseman; J. A. Montgomery; Jr.; T. Vreven; K. N. Kudin; J. C. Burant; J. M. Millam; S. S. Iyengar; J. Tomasi; V. Barone; B. Mennucci; M. Cossi; G. Scalmani; N. Rega; G. A. Petersson; H. Nakatsuji; M. Hada; M. Ehara; K. Toyota; R. Fukuda; J. Hasegawa; M. Ishida; T. Nakajima; Y. Honda; O. Kitao; H. Nakai; M. Klene; X. Li; J. E. Knox; H. P. Hratchian; J. B. Cross; V. Bakken; C. Adamo; J. Jaramillo; R. Gomperts; R. E. Stratmann; O. Yazyev; A. J. Austin; R. Cammi; C. Pomelli; J. W. Ochterski; P. Y. Ayala; K. Morokuma; G. A. Voth; P. Salvador; J. J. Dannenberg; V. G. Zakrzewski; S. Dapprich; A. D. Daniels; M. C. Strain; O. Farkas; D. K. Malick; A. D. Rabuck; K. Raghavachari; J. B. Foresman; J. V. Ortiz; Q. Cui; A. G. Baboul; S. Clifford; J. Cioslowski; B. B. Stefanov; G. Liu; A. Liashenko; P. Piskorz; I. Komaromi; R. L. Martin; D. J. Fox; T. Keith; M. A. Al-Laham; C. Y. Peng; A. Nanayakkara; M. Challacombe; P. M. W. Gill; B. Johnson; W. Chen; M. W. Wong; C. Gonzalez; and J. A. Pople. Gaussian03, Revision C.02; Gaussian, Inc., 2004.
(59) Blowers, P., Zheng, X.; Zhang, N. *Molecular Simulation* **2005**, *accepted*.
(60) Zheng, X., Blowers, P. *J. Phys. Chem. A* **2005**, *accepted*.
(61) Zheng, X., Blowers, P. *Molecular Simulation* **2005**, *31*, 615.
(62) Lei, W., Zhang, R.; Molina, L. T.; Molina, M. J. *J. Phys. Chem. A* **2002**, *106*, 6415.
(63) Perez-Casany, M. P., Nebot-Gil, I.; Sanchez-Marin, J. **2000**.
(64) Perez-Casany, M. P., Sanchez,-Marin, J.; Nebot-Gil, I. *J. Am. Chem. Soc.* **2000**, *122*, 11585.
(65) Yamaguchi, Y., Frisch, M.; Gaw, J.; Schaefer, H. F. III; Binkley, J. S. *J. Chem. Phys.* **1986**, *84*, 2262.
(66) Miller, M. D., Jensen, F., Chapman, O. L., Houk, K. N. *J. Phys. Chem.* **1989**, *93*, 4495.
(67) Bruns, R. E., Guadagnini, P. H.; Scarminio, E. S.; de Barros Neto, B. *J. Molec. Struct. (Theochem)* **1997**, *394*, 197.
(68) In *http://chemistry.umeche.maine.edu/Modeling/DFT.html*.
(69) Halls, M. D., Schlegel, H. B. *J. Chem. Phys.* **1998**, *109*, 10587.
(70) Jungkamp, T. P. W., J. N. Smith; Seinfeld, J. H. *J. Phys. Chem. A* **1997**, *101*, 4392.
(71) Blowers, P., Zheng, X.; Homan, K. *Chem. Engr. Commun.* **2003**, *190*, 1233.
(72) Mayer, P. M., C. J. Parkinson, D. M. Smith, Radom, L. *J. Chem. Phys.* **1998**, *108*, 604.
(73) da Silva, J. B. P. *J. Braz. Chem. Soc.* **2000**, *11*, 219.
(74) Hou, H., Wang, B.; Gu, Y. *J. Phys. Chem. A* **2000**, *104*, 1570.
(75) Kharroubi, M., de Sainte Claire, P. *J. Phys. Chem. A* **2003**, *107*, 4483.
(76) Pacey, P. D. *J. Chem. Educ.* **1981**, *58*, 612.
(77) Steinfeld, J. I., Francisco, J.S.; Hase, W.L *Chemical Kinetics and Dynamics*; Prentice-Hall: New Jersey, 1999.

(78) Duncan, W. T., Bell, R. L.; Truong, T. N. *J. Comp. Chem.* **1998**, *19*, 1039.
(79) Lin, H., Burger, H.; Mkadmi, E. B.; He, S.-G,; Yuan, L.-F.; Breidung, J.; Thiel, W.; Huet, T. R.; Demaison, J. *J. Chem. Phys.* **2001**, *115*, 1378.
(80) Espinosa-Garcia, J. *J. Phys. Chem. A* **2002**, *106*, 5686.
(81) Martell, J. M., Boyd, R. J. *J. Phys. Chem.* **1995**, *99*, 13402.
(82) Daub, C. D., Henry, B. R.; Sage, M. L.; Kjaergaard, H. G. *Can. J. Chem.* **1999**, *77*, 1775.
(83) He, S.-G., Zheng, J.-J.; Hu, S.-M.; Lin, H.; Ding, Y.; Wang, X.-H.; Zhu, Q.-S. *J. Chem. Phys.* **2001**, *6*, 7018.
(84) Henry, B. R., Kjaergaard, H. G. *Can. J. Chem.* **2002**, *80*, 1635.
(85) Takahashi, K., Sugawara, M.; Yabushita, S. *J. Phys. Chem. A* **2002**, *106*, 2676.
(86) Papasavva, S., Tai, S.; Esslinger, A.; Illinger, K. H.; Kenny, J. E. *J. Phys. Chem.* **1995**, *99*, 3438.
(87) Freckleton, R. S., Pinnock, S.; Shine, K. P. *J. Quant. Spectroscopy Radiat. Transfer* **1996**, *55*, 763.
(88) Patten, K. O., Jr., Li, Z.; Wuebbles, D. J. *J. Geophys. Res.* **2000**, *105*, 11625.
(89) Prather, M., Spivakovsky, C. M. *J. Geophys. Res. Atmos.* **1990**, *95*, 18723.
(90) DeMore, W. B. *J. Phys. Chem.* **1996**, *100*, 5813.
(91) Prinn, R. G., Weiss, R. F.; Miller, B. R.; Huang, J.; Alyea, F. N.; Cunnold, D. M.; Fraser, P. J.; Hartley, D. E.; Simmonds, P. E. *Science* **1995**, *269*, 187.
(92) Donald, K. J., Bohm, M. C.; Lindner, H. J. *J. Mol. Struct. (Theochem)* **2004**, *710*, 1.
(93) Hirota, E. *J. Molec. Spectrosc.* **1978**, *71*, 145.
(94) Luke, B. T., Loew, G. H.; McLean, A. D. *J. Am. Chem. Soc.* **1987**, *109*, 1307.
(95) Hirota, E., Tanaka, T.; Sakakibara, A.; Ohashi, Y.; Morino, Y. *J. Molec. Spectrosc.* **1970**, *34*, 222.
(96) Lide, D. R. J. *J. Am. Chem. Soc.* **1952**, *74*, 3548.
(97) Russell, A. J., Spackman, M. A. *Molec. Phys.* **2000**, *98*, 633.
(98) Afeefy, H. F., Liebman, J. F.; Stein, S. E. Neutral Thermochemical Data. In *NIST Chemistry WebBook, NIST Standard Reference Database Number 69*; Mallard, E. P. J. L. a. W. G., Ed.; National Institute of Standards and Technology: Gaithersburg MD, 2005.
(99) Pickard, J. M., Rodgers, A. S. *Int. J. Chem. Kinet.* **1983**, *15*, 569.
(100) Lee, E. P. F., Dyke, J. M; Mayhew, C. A. *J. Phys. Chem. A* **1998**, *102*, 8349.
(101) McMillen, D. F., Golden, D. M. *Ann. Rev. Phys. Chem.* **1982**, *33*, 493.
(102) Korchowiec, J. *J. Phys. Org. Chem.* **2002**, *15*, 524.
(103) Yamataka, H., Nagase, S.; Ando, T.; Hanafusa, T. *J. Am. Chem. Soc.* **1986**, *108*, 601.
(104) Lee, W. T., Masel, R. I. *J. Phys. Chem.* **1996**, *100*, 10945.
(105) Lee, W. T., Masel, R. I. *J. Phys. Chem.* **1995**, *99*, 9363.
(106) Zheng, X., Blowers, P. *J. Molec. Catal. A: Chemical* **2005**, *accepted*.

List of Captions:

Figure 1a - The flow of information from experimental sources to reach global warming potential estimates.

Figure 1b - The flow of information from purely computational chemistry methods to reach global warming potential estimates.

Figure 2 - A comparison of predicted frequencies for CH_2F_2 compared to experimental results. All peak locations are reported in cm^{-1} and the results from this work have been scaled by 0.9613 as discussed in the methodology section. Other results that were scaled by an empirical factor are listed in Table S4.

Figure 3 - A comparison of predicted IR intensities for CH_2F_2 compared to experimental results. Three experimental works were averaged together and used as the experimental value for error estimates. Intensities for the 109, 1113 and 1178 peak were summed as some experiments were unable to resolve these peaks individually.

Figure 4 - A comparison of rate constants for the $CH_2F_2 + OH \rightarrow CHF_2 + H_2O$ predicted from theory at the CBS-RAD level using transition state theory including tunneling corrections to experimental results. k here is in units of $cm^3/mol\ sec$.

Figure 5 - A comparison of all computational rate constants for the $CH_2F_2 + OH \rightarrow CHF_2 + H_2O$ reaction compared to the experimental compilation of DeMore.

Figure 1a

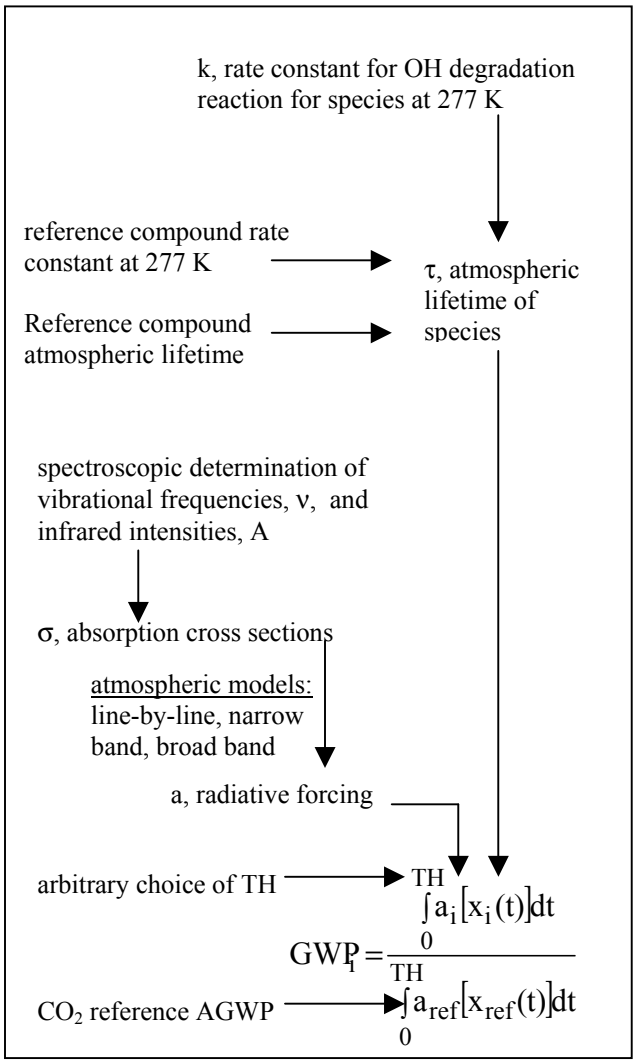
k, rate constant for OH degradation reaction for species at 277 K
reference compound rate constant at 277 K
τ, atmospheric lifetime of species
Reference compound atmospheric lifetime
spectroscopic determination of vibrational frequencies, ν, and infrared intensities, A
σ, absorption cross sections
atmospheric models: line-by-line, narrow band, broad band
a, radiative forcing
arbitrary choice of TH
$GWP_i = \frac{\int_0^{TH} a_i[x_i(t)]dt}{\int_0^{TH} a_{ref}[x_{ref}(t)]dt}$
CO_2 reference AGWP

Figure 1b

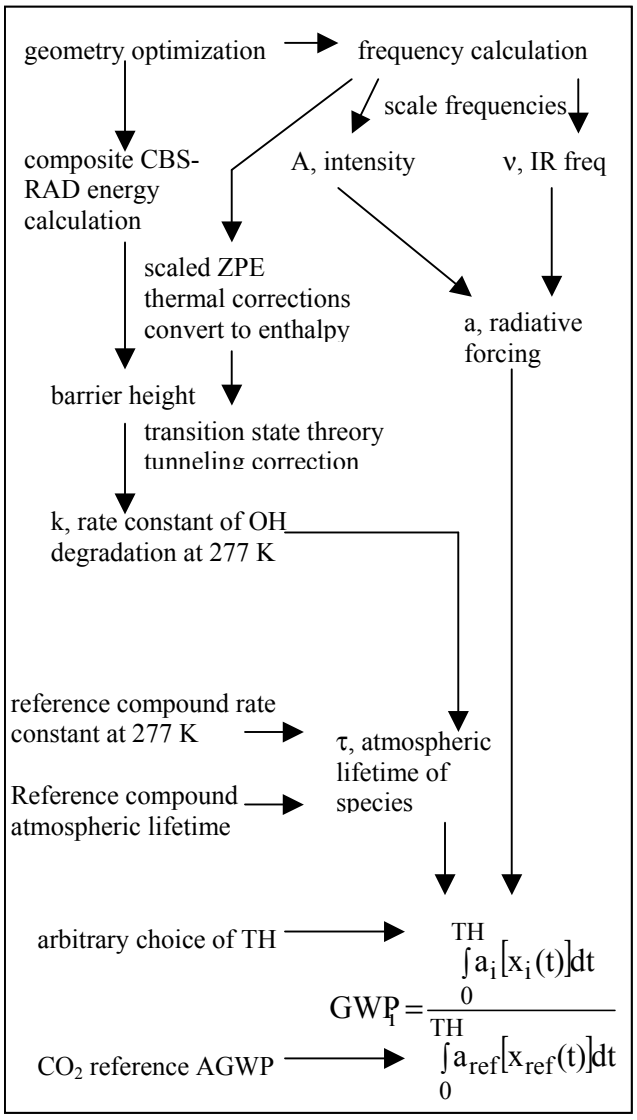
geometry optimization
frequency calculation
scale frequencies
composite CBS-RAD energy calculation
A, intensity
ν, IR freq
scaled ZPE
thermal corrections
convert to enthalpy
a, radiative forcing
barrier height
transition state threory
tunneling correction
k, rate constant of OH degradation at 277 K
reference compound rate constant at 277 K
τ, atmospheric lifetime of species
Reference compound atmospheric lifetime
arbitrary choice of TH
$GWP_i = \frac{\int_0^{TH} a_i[x_i(t)]dt}{\int_0^{TH} a_{ref}[x_{ref}(t)]dt}$
CO_2 reference AGWP

Figure 2

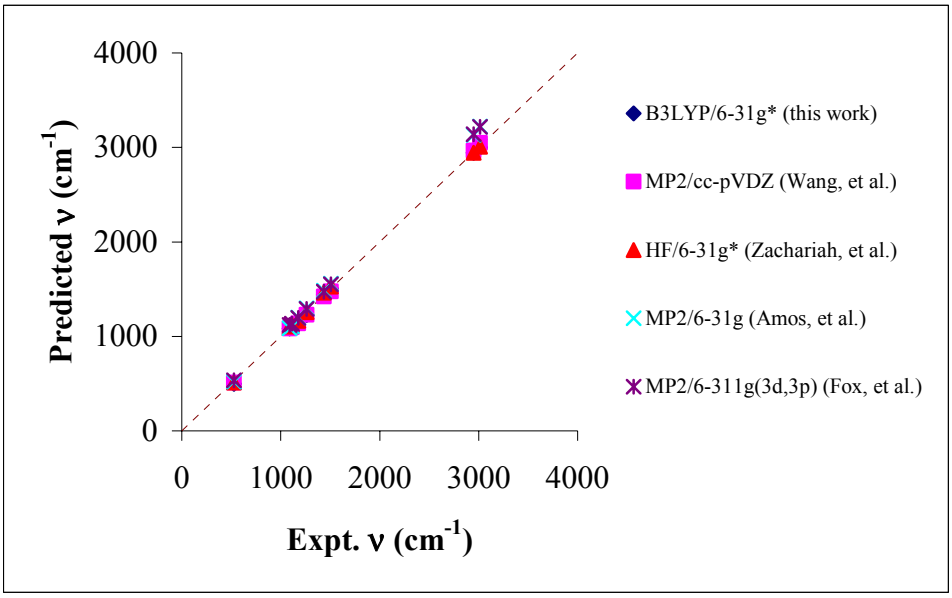

Wang, et al.[41], Zachariah, et al.[46], Amos, et al.[44], Fox, et al.[45]

Figure 3

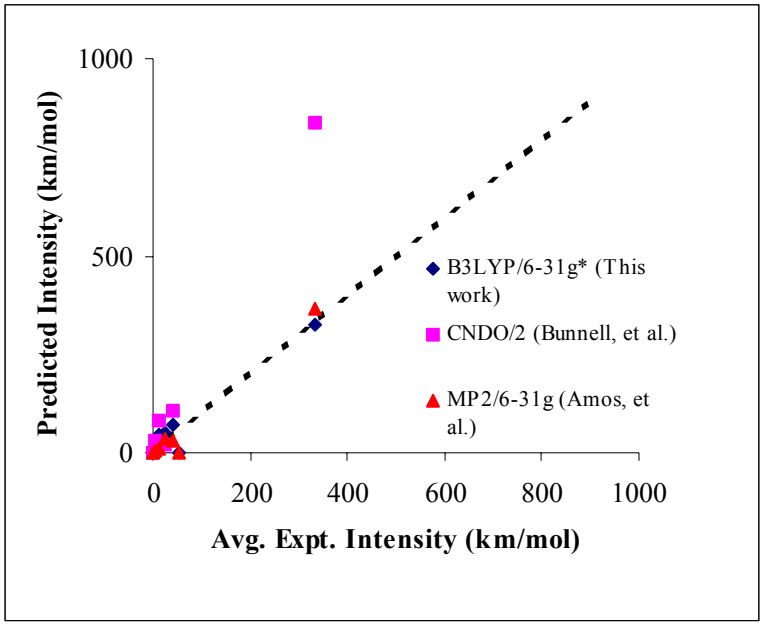

Bunnel, et al.[52], Amos, et al[44].

Figure 4

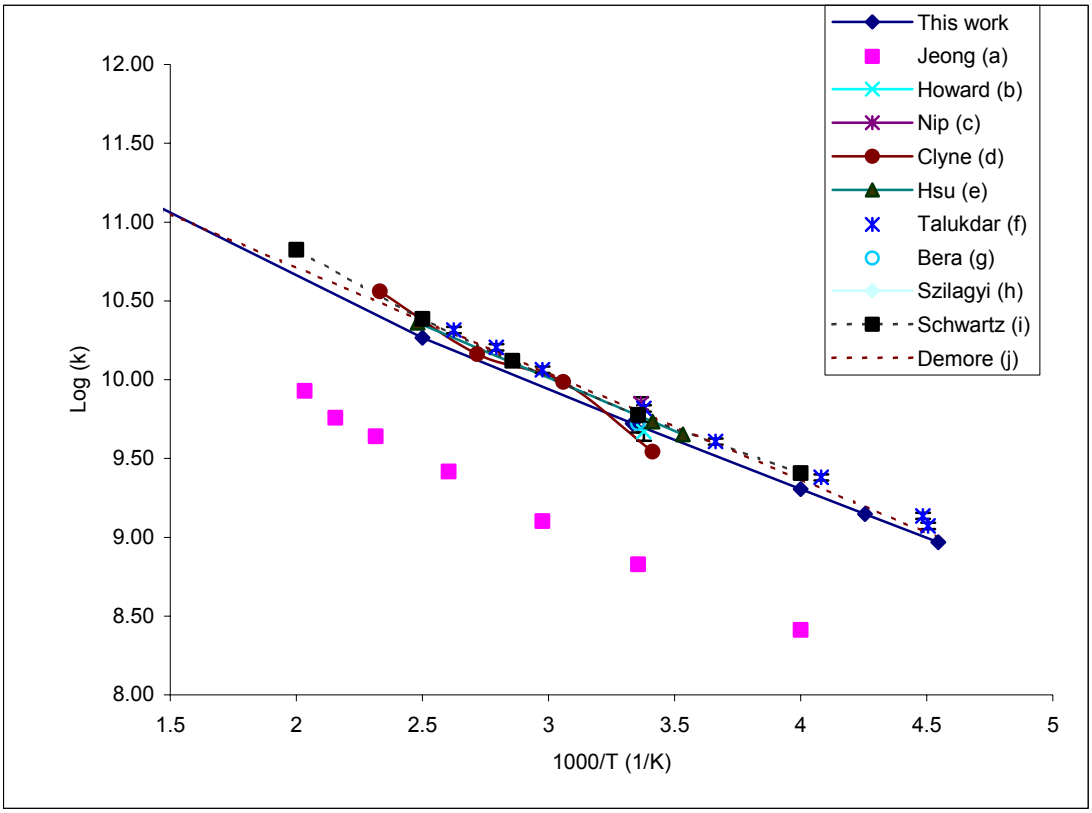

a ref [24], b ref [25], c [26], d [27],e [28], f [29], g [30], h [31], i [20], j[34].

Figure 5

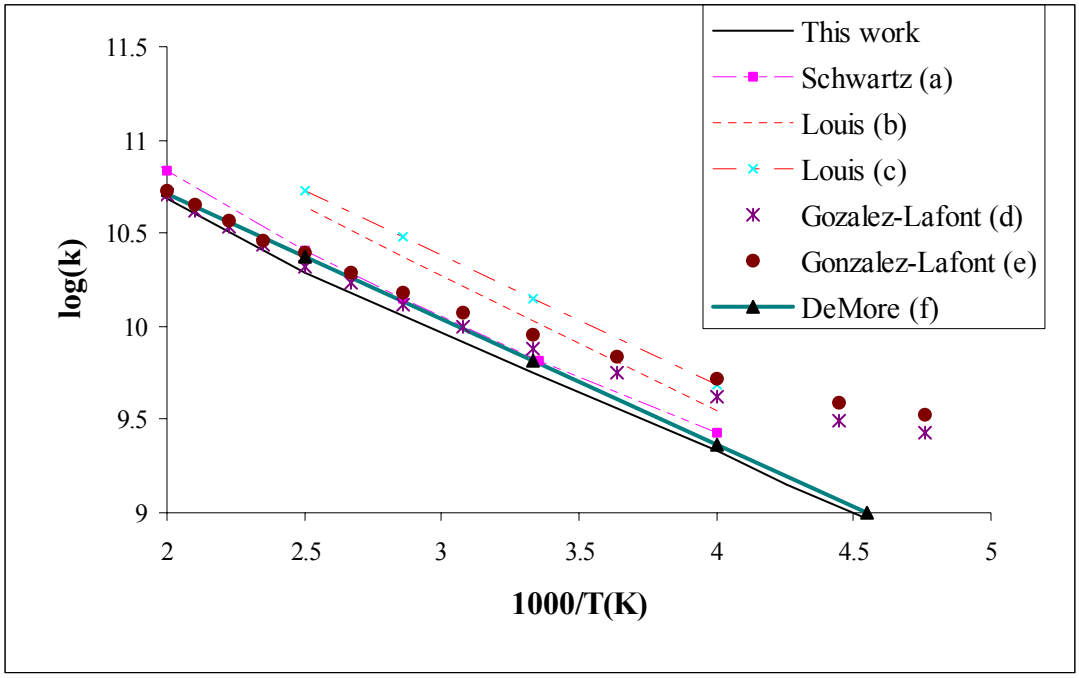

This work (CBS-RAD/B3LYP/6-31*), a ref [20] (G2/MP2/6-31g*), b ref[38] (PMP4(SDTQ)/6-311G(3df,2p), c ref [38] (PMP4(SDTZ)/6-311++g(2df,2pd)), d ref [39] (QCISD(T)/6-311++G(2df,p)//QCISD/6-311g(d,p)[QCISD/6-31g(d)]///PM3, e ref [39] (CCSD(T)//MP2/cc-pVTZ///PM3), f ref [34]